NASA

Technical Memorandum 80589

Passive Microwave Remote Sensing of Soil Moisture: The Effect of Tilled Row Structure

J. R. Wang, R. W. Newton,
and J. W. Rouse

JUNE 1979

National Aeronautics and
Space Administration

Goddard Space Flight Center
Greenbelt, Maryland 20771

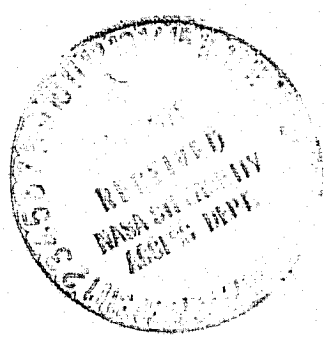

TM80311

PASSIVE MICROWAVE REMOTE SENSING OF SOIL MOISTURE: THE EFFECT OF TILLED ROW STRUCTURE

J. R. Wang,[1] R. W. Newton,[2] and J. W. Rouse[3]

June 1979

[1]Laboratory for Atmospheric Sciences, NASA Goddard Space Flight Center

[2]Remote Sensing Center, Texas A&M University, College Station, Texas

[3]Department of Electrical Engineering, University of Missouri, Columbia, Missouri

GODDARD SPACE FLIGHT CENTER
Greenbelt, Maryland

PASSIVE MICROWAVE REMOTE SENSING OF SOIL MOISTURE: THE EFFECT OF TILLED ROW STRUCTURE

ABSTRACT

The tilled row structure is known to be one of the important factors affecting the observations of the microwave emission from a natural surface. Measurements of this effect were carried out with both L- and X-band radiometers mounted on a mobile truck on a bare 40 m x 45 m row tilled field. The soil moisture content during the measurements ranged from ~ 10% to ~ 30% by dry weight. The results of these measurements showed that the variations of the antenna temperatures with incident angle θ changed with the azimuthal angle a measured from the row direction. In particular, at $\theta = 0°$ and $a \neq 45°$, the observed horizontally and vertically polarized antenna temperatures, $T_{BH}(\theta, a)$ and $T_{BV}(\theta, a)$, were not equal. In general, $T_{BH}(0°, a) > T_{BV}(0°, a)$ when $0° \leq a < 45°$ and $T_{BH}(0°, a) < T_{BV}(0°, a)$ when $45° < a \leq 90°$. The difference between $T_{BH}(0°, a)$ and $T_{BV}(0°, a)$ was observed to decrease with a approaching 45° and/or with soil moisture content.

A numerical calculation based on a composite surface roughness – a small scale RMS height variations superimposed on a large periodic row structure – was made and found to predict the observed features within the model's limit of accuracy. It was concluded that the difference between T_{BV} $(0°, \alpha)$ and T_{BH} $(0°, \alpha)$ was due to the change in the local angle of field emission within the antenna field of view caused by the large-scale row structure.

CONTENTS

	Page
1. INTRODUCTION	1
2. THE FIELD MEASUREMENTS AND RESULTS	2
3. DATA ANALYSIS AND INTERPRETATION	5
4. A NUMERICAL CALCULATION	8
5. DISCUSSION	11
6. CONCLUSION	12
APPENDIX A	13
REFERENCES	15

PASSIVE MICROWAVE REMOTE SENSING OF SOIL MOISTURE: THE EFFECT OF TILLED ROW STRUCTURE

1. INTRODUCTION

The microwave emission from an agricultural field depends on many factors. These factors include the frequency of emission, soil moisture content and profile, soil temperature profile, soil texture, surface roughness, vegetation cover, and row structure. The frequency dependence as well as the effects of moisture content and temperature profile on the microwave emission from soils have been studied in some detail by Schmugge, Gloersen, Wilheit, and Geiger (1), Njoku and Kong (2), Schmugge, Wilheit, Webster, and Gloersen (3) and by Newton (4). The results of laboratory measurements (4,5,6) have demonstrated the effects of soil texture on the complex dielectric permittivity which in turn affect the microwave emissivity of soils. The results of field experiments (7) showed that the unique relationship between the measured brightness temperature and soil moisture content was much improved when soil types were quantified. The effect of surface roughness on the microwave emission from soils have been explored by Newton (4) and, more recently, analyzed in some length by Choudhury, Schmugge, Newton, and Chang (8). However, the effects of vegetation cover and the field row structure have been studied only qualitatively by Sibley (9) and by Newton (4), although the contribution from these factors to the microwave emission of soils have long been recognized.

In this paper, the effect of the row structure on the microwave emission from a bare agriculture field is reported. The data used in the study were obtained from the Joint Soil Moisture Experiment (JSME) carried out in July 1975 (10). The measurements were made with both L-band (1.42 GHz) and X-band (10.69 GHz) radiometers mounted on a mobile truck. The observed data at both frequencies showed a definite difference in the variations of the antenna temperature with angle of incidence depending on whether the antennas were scanning preferentially parallel or perpendicular to the row direction. In particular, the antenna temperature at nadir was observed to be higher in the horizontal polarization than in the vertical polarization when the antenna scanning was parallel to the row direction. As the antenna scanning was made perpendicular to the row direction, the vertically polarized antenna temperature was observed to be higher than the horizontally polarized

one. These differences in the vertically and horizontally polarized antenna temperatures at nadir were enhanced with the increase in the soil moisture content. It is suggested that the changes in the orientations of the electromagnetic fields of emission due to the presence of the row structure are responsible for the observed phenomena. A simple calculation based on the variation of the electromagnetic field orientations and the geometry of the row structure is made and found to be able to account for most of the observed results.

2. THE FIELD MEASUREMENTS AND RESULTS

The truck measurements and the ground truth data collection were carried out over two fields in the Texas A&M University Research Farm in Burleson County, Texas. The soil within these fields is Miller Clay which is composed of 62 percent clay (by weight), 35 percent silt and 3 percent sand. Both fields were plowed with rows running east-west. Field A is bare soil and Field B is planted with cotton. Only the results from the bare field measurements will be discussed in this paper. The average height and width for a row in the bare soil field were 20 cm and 95 cm, respectively.

The radiometric measurements were made for both horizontal and vertical polarizations at both 1.42 GHz and 10.69 GHz frequencies. The beamwidths for the X-band and L-band antennas were about 6° and 15°, respectively. Both antennas were maintained at a constant height of ~14 m above the field during all measurements. Measurements were made at incident angles of 0°, 20°, 35°, and 50° and at the azimuthal angles of 0°, 30°, 45°, 60°, and 90° with respect to the row direction. The functioning of both radiometers was checked by measuring the responses to water and sky. The entire field measurements were carried out on the 16th, 17th, 18th, 20th, 21st, 24th, and 25th of July 1975. The details of the ground truth acquisition, sensor calibration, and data reduction were described by Newton and Tesch (10). The following analysis is based on the data from that report.

Figure 1 shows the results of the L-band measurements on July 16, 1975, with the antenna temperature plotted as a function of incident angle θ. The average soil moisture content during the measurements varied from ~26.5% at 0-1 cm to 21.4% at 9-15 cm. Four scans with azimuthal angles (α) of 0°, 30°, 60°, and 90° with respect to row direction were made, in sequential order, around 12:12 p.m., 14:26 p.m., 10:18 a.m., and 7:55 a.m. The spread in the antenna temperatures from one azimuthal scan to another was partly due to the changes of soil temperature and moisture content from early morning to late afternoon, as these parameters were observed to change drastically

with diurnal cycle (11). It is shown in the next section that when the observed antenna temperatures were normalized to these parameters, the spread was reduced appreciably.

It is clear from Figure 1 that, for each scan with azimuthal angle α (measured from row direction) at $\theta = 0°$, the observed antenna temperatures of vertical ($T_{BV}(\theta, \alpha)$) and horizontal ($T_{BH}(\theta, \alpha)$) polarizations do not coincide. For scan with $\alpha = 0°$, $T_{BH}(0°, 0°)$ is ~14°K higher than $T_{BV}(0°, 0°)$. For $\alpha = 30°$, the difference between $T_{BH}(0°, 30°)$ and $T_{BV}(0°, 30°)$ still persists, but the magnitude of the difference is reduced to ~7°K. For the remaining scans of $\alpha = 60°$ and $\alpha = 90°$, $T_{BV}(0°, 60°)$ and $T_{BV}(0°, 90°)$ are observed to be higher than $T_{BH}(0°, 60°)$ and $T_{BH}(0°, 90°)$ respectively. The magnitude of $T_{BV}(0°, \alpha) - T_{BH}(0°, \alpha)$ increases from ~9°K at $\alpha = 60°$ to ~17°K at $\alpha = 90°$. This systematic variation of the differences in $T_{BH}(0°, \alpha)$ and $T_{BV}(0°, \alpha)$ with α is not limited to the measurements made on July 16, 1975, but is observable on all of the other measurements on Field A reported by Newton and Tesch (10). Figure 2 shows the similar plot for the data obtained on July 25, 1975 when the soil moisture ranges from ~9.6% at 0 - 1 cm to ~28.3% at 9 - 15 cm. $T_{BH}(0°, 0°)$ is observed to be higher than $T_{BV}(0°, 0°)$ by ~6°K while $T_{BH}(0°, 90°)$ is smaller than $T_{BV}(0°, 90°)$ by ~7°K. When $\alpha = 45°$, the difference between $T_{BH}(0°, 45°)$ and $T_{BV}(0°, 45°)$ is only ~2.2°K. The scans at $\alpha = 45°$ were also made on July 21, 22, and 24. In all of these measurements the differences between $T_{BH}(0°, 45°)$ and $T_{BV}(0°, 45°)$ were found to be $\leq$2°K. The differences of ~2°K are comparable with the precision of the measurements and are consistent with $T_{BH}(0°, 45°) \simeq T_{BV}(0°, 45°)$. Thus, the measurements at L-band show a definite pattern for the antenna temperature difference $T_{BH}(0°, \alpha) - T_{BV}(0°, \alpha)$. This difference decreases as α increases from 0° to 90°, changing sign at $\alpha = 45°$. A comparison between Figures 1 and 2 also suggests that for the same α, the magnitude of $T_{BH}(0°, \alpha) - T_{BV}(0°, \alpha)$ decreases as soil moisture content decreases.

Another feature observed from the variation of $T_{BH}(\theta, \alpha)$ and $T_{BV}(\theta, \alpha)$ with θ in Figure 1 is that the steepness of the $T_{BV}(\theta, \alpha)$ vs. θ curves decreases as α increases from 0° to 90°. This trend is apparent especially for the $T_{BV}(\theta, \alpha)$ vs. θ curves. For $\alpha = 0°$, $T_{BV}(\theta, 0°)$ increases from ~239°K at $\theta = 0°$ to ~265°K at $\theta = 50°$. $T_{BV}(\theta, 60°)$ increases from ~243°K to ~252°K over the same θ range. The $T_{BV}(\theta, 90°)$ vs. θ curve appears to be flat for all θ. For the $T_{BH}(\theta, \alpha)$ vs. θ curves, the change in the steepness with α is not as drastic. Note that $T_{BH}(\theta, 0°)$ decreases from ~253°K at $\theta = 0°$ to ~214°K at $\theta = 50°$, a drop of 39°K. The magnitude of this drop is reduced to ~32°K over

the same θ range when $a = 90°$. This general trend of the flattening in the $T_{BV}(\theta, a)$ or $T_{BH}(\theta, a)$ vs. θ curves with increase in a can also be seen in Figure 2, although the rate of flattening is not as drastic compared to the case of $T_{BV}(\theta, a)$ vs. θ curves in Figure 1.

Both of the features displayed by the L-band measurement results above are also observed in the X-band data to some extent. Figure 3 shows the results of the X-band measurements on July 16, 1975. Again the large spread in the brightness temperatures from one azimuthal scan to another is partly due to the increase in soil temperature and the decrease in soil moisture from early morning to late afternoon. Note that $T_{BH}(0°, a) - T_{BV}(0°, a)$ for $a = 0°$, 30°, 60°, and 90° are approximately 10°K, 5°K, −15°K, and −24°K, which follows the general pattern set by the L-band measurement results shown in Figure 1. The variation of $T_{BV}(\theta, a)$ vs. θ are different from those observed in the L-band data, however. $T_{BV}(\theta, 0°)$ increases only slightly from ~237°K at $\theta = 0°$ to ~245°K at $\theta = 50°$. For $a = 30°$, 60°, and 90°, $T_{BV}(\theta, a)$ decreases with θ. $T_{BV}(\theta, 90°)$ drops by about 11°K from ~229°K at $\theta = 0°$ to ~218°K at $\theta = 50°$. The decreases in $T_{BH}(\theta, a)$ from $\theta = 0°$ to $\theta = 50°$ are similar to those displayed by L-band data. The decrease in $T_{BH}(\theta, 0°)$ and $T_B(\theta, 30°)$ is ~30° – 35°K over the θ range of 0° – 50°, while the drop in $T_{BH}(\theta, 60°)$ and $T_{BH}(\theta, 90°)$ is only ~20° – 25°K.

Clearly, the variations in $T_{BV}(\theta, a)$ and $T_{BH}(\theta, a)$ with a shown in Figures 1, 2, and 3 for both L-band and X-band measurements are definitely associated with the effect of the row structure. For all the L-band measurements carried out in the JSME program in July 1975, the general features of $T_{BH}(\theta, a)$ and $T_{BV}(\theta, a)$ variations with a discussed above are consistently present, although the magnitude of these variations changes with soil moisture content. For the X-band measurements, on the other hand, there are some exceptions. These exceptional cases were included in Figure 4 where the values of $T_{BH}(0°, a) - T_{BV}(0°, a)$ are plotted as a function of a. It is noted that for $a = 0°$ and 30°, there are four cases where the values of $T_{BH}(0°, a) - T_{BV}(0°, a)$ are negative. These few cases are not in accordance with the general features observed in Figures 1, 2, and 3.

From an examination of the data compiled by Newton and Tesch (10), two possible sources of uncertainty in the X-band measurements are found which may cause the deviation from the observed features associated with the effect of row structure. First, the standard deviations of the observed antenna temperatures are generally 3-4 times higher in the X-band measurements than in the L-band measurements. This suggests a noisier X-band radiometer compared to the L-band radiometer.

Secondly, the X-band water calibration measurements at nadir showed a 5° - 15°K higher antenna temperature output in vertical polarization than in horizontal polarization. If this affect is not taken into account properly, the values of $T_{BH}(0°, a) - T_{BV}(0°, a)$ would shift to the negative side as implied by the pattern of Figure 4. Nevertheless, the effect of the row structure is clearly demonstrated by the general decrease of $T_{BH}(0°, a) - T_{BV}(0°, a)$ with a. In the following data analysis and interpretation, the emphasis will be placed on the L-band measurement results.

3. DATA ANALYSIS AND INTERPRETATION

Most of the observed systematic variation of $T_{BH}(\theta, a)$ and $T_{BV}(\theta, a)$ with a described in the previous section can be understood by a simple geometric consideration between the measurement system and the field row direction. Figure 5 shows a sketch of the field-antenna configuration. The orientations of both the horizontally and vertically polarized fields as seen by the radiometer antenna, $E_H(0°, a)$ and $E_V(0°, a)$, are shown in the figure for $a = 0°$ and 90°. The unit normal vector and incident angle to the tangential plane of a small local region are indicated by $\hat{n}_i$ and γ_i respectively. The horizontally and vertically polarized fields of emission from the small local region are given by $\&_H(\gamma_i)$ and $\&_V(\gamma_i)$. Note that the local angle of field emission is not equal to the antenna incident angle θ. It is clear that, for $a = 90°$, $\&_V(\gamma_i)$ and $\&_H(\gamma_i)$ contributes to $E_V(0°, 90°)$ and $E_H(0°, 90°)$ respectively. On the other hand, when $a = 0°$, the contributions to $E_V(0°, 0°)$ and $E_H(0°, 0°)$ comes from $\&_H(\gamma_i)$ and $\&_V(\gamma_i)$ respectively. An immediate consequence from these considerations is that $E_V(0°, 0°) = E_H(0°, 90°)$ and $E_H(0°, 0°) = E_V(0°, 90°)$. Since the antenna temperature is proportional to the square of the electric fields, $T_{BV}(0°, 0°) = T_{BH}(0°, 90°)$ and $T_{BH}(0°, 0°) = T_{BV}(0°, 90°)$ under the same field conditions.

Observations in the past (1,4) have shown that, for a flat bare soil field, $T_{BH}(\theta, a)$ decreases with θ indefinitely, while $T_{BV}(\theta, a)$ increases with θ up to the Brewster's angle. The rate of change of $T_{BH}(\theta, a)$ or $T_{BV}(\theta, a)$ with θ depends on soil moisture content and surface roughness, being more rapid for a smoother surface or higher moisture content. Referring to Figure 5, the microwave emission from a local region with a non-zero γ_i would be higher for the vertically polarized component than for the horizontally polarized component. When summed over the footprint of a radiometer

looking at nadir, $T_{BH}(0°, 0°)$ and $T_{BV}(0°, 90°)$ are expected to be higher than $T_{BV}(0°, 0°)$ and $T_{BH}(0°, 90°)$; This is in accordance with the observed data presented in the previous section. The larger magnitudes in $T_{BH}(0°, 0°) - T_{BV}(0°, 0°)$ and $T_{BV}(0°, 90°) - T_{BH}(0°, 90°)$ when the field was wet on July 16, compared to those obtained from other measurements when the field was dry, are also a direct consequence of this reasoning.

To substantiate the general picture described above, all the measurements made at $a = 0°$ and 90° are analyzed in more detail below. Table 1 shows the dates and times of these measurements as well as the informations on azimuthal angles, polarizations, antenna temperatures, soil temperatures, soil moisture contents and the normalized antenna temperatures. Both moisture contents and soil temperatures are average values over the top 2-cm layer. Since both of these parameters could change rapidly with time (11), only the values measured within ~±2 hours of the times of the radiometric measurements were included in the averaging process. The normalized antenna temperature $T_{NP}(\theta, a)$ is defined as

$$T_{NP}(\theta, a) = \frac{T_{BP}(\theta, a)}{T_G} \tag{1}$$

where the subscript p stands for either H or V, and T_G is the measured soil temperature. The normalized antenna temperatures $T_{NH}(0°, 0°)$, $T_{NV}(0°, 0°)$, $T_{NH}(0°, 90°)$, and $T_{NV}(0°, 90°)$, the soil moisture contents for measurements at $a = 0°$ and $a = 90°$, and the differences $T_{NH}(0°, 0°) - T_{NV}(0°, 90°)$ and $T_{NV}(0°, 0°) - T_{NH}(0°, 90°)$ are plotted vs. times of the measurements in Figure 6. No ground truth data collections were made for the $a = 0°$ measurements between 12-15 P.M. local time on July 24 and 25. The soil temperature obtained between 10-12 A.M. for the $a = 45°$ measurements were used to normalize the measured $a = 0°$ antenna temperatures.

From this figure the soil moisture content is observed to decrease with time from ~30% on July 16 to ~11% on July 25. The four sets of the normalized temperatures increase with time from a range of 0.73 - 0.83 to a range of 0.89 - 0.93 range over the same time period. Three distinct features are present in the four sets of normalized antenna temperature data. First, in each day of the measurement, $T_{NH}(0°, 0°) > T_{NV}(0°, 0°)$ and $T_{NV}(0°, 90°) > T_{NH}(0°, 90°)$. Secondly, with the exception of the data on July 16, $T_{NH}(0°, 0°) \simeq T_{NV}(0°, 90°)$ and $T_{NV}(0°, 0°) \simeq T_{NH}(0°, 90°)$. Thirdly, the magnitudes of $T_{NH}(0°, 0°) - T_{NV}(0°, 0°)$ and $T_{NV}(0°, 90°) - T_{NH}(0°, 90°)$ decrease with time from

~0.10 on July 16 to ~0.4 on July 25. All these features are consistent with the microwave emission processes shown in Figure 5.

The differences between $T_{NV}(0°, 0°)$ and $T_{NH}(0°, 90°)$ and between $T_{NH}(0°, 0°)$ and $T_{NV}(0°, 90°)$ on July 16 (also see Figure 1) is primarily due to the change in soil moisture contents between the $a = 0°$ and $a = 90°$ scans. The change in the soil moisture between the two scans was ~4%, while $T_{NV}(0°, 0°) - T_{NH}(0°, 90°) = 0.043$ and $T_{NH}(0°, 0°) - T_{NV}(0°, 90°) = 0.026$. Refering to the slopes of the plot between the normalized antenna temperatures and moisture content in Figure 7, the differences of 0.043 and 0.026 in the brightness temperatures can be entirely accounted for by the 4% moisture change. The moisture changes between the two different azimuthal scans in the measurements on July 17, 18, 20, 22, 24, and 25 could also be responsible for the observed trend in the plot of $T_{NV}(0°, 0°) - T_{NH}(0°, 90°)$ and $T_{NH}(0°, 0°) - T_{NV}(0°, 90°)$ vs. time, although some of these differences were comparable to the precision of the measurements. Note that the moisture contents during the $a = 0°$ scan are smaller than those during the $a = 90°$ scan on July 18, 20, 21, 24, and 25. Both $T_{NV}(0°, 0°) - T_{NH}(0°, 90°)$ and $T_{NH}(0°, 0°) - T_{NV}(0°, 90°)$ are found to be positive, as expected, on those days. The measurements on July 17 and 22 were carried out such that the moisture contents during $a = 0°$ scan were higher than those during the $a = 90°$ scan. Both $T_{NV}(0°, 0°) - T_{NH}(0°, 90°)$ and $T_{NH}(0°, 0°) - T_{NV}(0°, 90°)$ on those days are negative, implying the association of the lower brightness temperatures with higher soil moisture contents. This effect strongly suggests the importance of the simultaneous acquisition of the radiometric measurements and the ground truth.

The observed values of $T_{NV}(0°, 0°)$ and $T_{NH}(0°, 90°)$ were plotted as a function of the soil moisture content W in Figure 7. A linear regression analysis of all the data points gave a correlation coefficient of 0.92. A similar regression was also performed for the data of $T_{NH}(0°, 0°)$ and $T_{NV}(0°, 90°)$ and the result was shown as a dashed line in Figure 7. The correlation coefficient was found to be 0.89 in this case. Three features are clearly displayed by this figure. First, the data points for $T_{NV}(0°, 0°)$ and $T_{NH}(0°, 90°)$ are well mixed (same for $T_{NH}(0°, 0°)$ and $T_{NV}(0°, 90°)$), again showing the equivalence between $T_{NV}(0°, 0°)$ and $T_{NH}(0°, 90°)$ measurements. Secondly, the slope of the $T_{NV}(0°, 0°)$ and $T_{NH}(0°, 90°)$ vs. W regression is steeper than that of the $T_{NH}(0°, 0°)$ and $T_{NV}(0°, 90°)$ vs. W regression. This suggests that the nadir viewing measurements with

electric field parallel to the row direction have a better moisture sensitivity compared to those with electric field perpendicular to the row direction. Thirdly, the difference between the two regression lines increases with W. This implies a stronger effect due to row structure at higher soil moisture content. The very similar intercept values between the two regression lines at W = 0% strongly suggests that the effect of row structure is negligible in the radiometric measurements when the soil is dry.

4. A NUMERICAL CALCULATION

A bare row tilled terrain can be regarded as a composite rough surface characterized by a uniform small-scale RMS surface height variation superimposed on the large-scale periodic row structure. The small-scale roughness effect at $\theta = 0°$ has been studied with a one-parameter model by Choudhury et al. (8). They showed that the gross effect of the small-scale surface roughness can be incorporated by modifying the smooth surface reflectivity $r_{OP}(\theta = 0°)$, i.e.,

$$r_p(\theta = 0°) = r_{OP}(\theta = 0°) \exp(-h) \qquad (2)$$

A rigorous calculation of $r_p(\theta)$ requires integration over a half space knowing the surface roughness statistics (4). Because of the lack of exact surface statistics, a simple empirical approach is adopted here. A comparison of the normalized antenna temperatures from measurements by Newton (12) on smooth, medium rough and rough surfaces of Miller Clay was made at $\theta = 0°$, 20°, 35° and 50°. For each θ, calculations of the normalized antenna temperature using Wilheit's layered dielectric model (13) were made with measured soil moisture and temperature profiles. The roughness parameter h was adjusted so that the calculated results reflected the necessary changes in the measured normalized antenna temperatures from smooth to medium rough or rough surfaces. It was found that there was only a slight dependence of h on θ over 0° – 50° range. For simplicity a constant h for all θ is assumed in the following calculations.

As shown in Figure 8, the antenna temperatures from a small area element ΔA_i, $T_{BH}(\gamma_i)$ and $T_{BV}(\gamma_i)$, are calculated from Wilheit's model with reflectivity $r_p(\gamma_i)$ given by Eq. (2). The antenna temperatures seen by a radiometer at incident angle θ and azimuthal angle α, $T_{BH}(\theta, \alpha)$ and $T_{BV}(\theta, \alpha)$, are the weighted sum of $T_{BH}(\gamma_i)$ and $T_{BV}(\gamma_i)$ over the footprint of the sensor. θ and γ_i are generally different. θ is the angle between the antenna's line of sight and the vertical axis, while γ_i is the angle between the antenna's line of sight and the local normal to ΔA_i.

The spatial variations of the large-scale periodic row structure associated with the 1975 JSME field measurements are approximately deterministic. From observations on several row cross sections taken at different places of the field (4), the spatial variations of the tilled rows could be approximately expressed in terms of a simple sinusoidal function. The form of the sinusoidal function and the detail derivation of the antenna temperatures, $T_{BH}(\theta, a)$, seen by a radiometer are given in Appendix A. The results are:

$$T_{BH}(\theta, a) = \frac{\sum_{i=1}^{N} \frac{(T_{BH}(\gamma_i)A^2 + T_{BV}(\gamma_i)B^2}{\sin^2\gamma_i} G(\phi_i)\Delta S_i}{\sum_{i=1}^{N} G(\phi_i)\Delta S_i} \tag{3}$$

$$T_{BV}(\theta, a) = \frac{\sum_{i=1}^{N} \frac{(T_{BH}(\gamma_i)C^2 + T_{BV}(\gamma_i)D^2)}{\sin^2\gamma_i} G(\phi_i)\Delta S_i}{\sum_{i=1}^{N} G(\phi_i)\Delta S_i} \tag{4}$$

The solid angle ΔS_i subtended by ΔA_i at the radiometer antenna and the antenna pattern $G(\phi_i)$ are given by

$$\Delta S_i = \frac{\Delta X_i \Delta Y_i \cos\gamma_i}{R_i^2 \cos\beta_i} \tag{5}$$

$$G(\phi_i) = \exp\left(-\frac{\phi_i^2}{\Delta\phi^2 \ln 2}\right) \tag{6}$$

where R_i is the distance from the antenna to ΔA_i, ϕ_i is the angle between line of sight defined by θ and R_i. $\Delta\phi \simeq 15°$ is the 3-db antenna beamwidth. A, B, C, and D are coefficients depending on θ, a, γ_i, θ_i, β_i and a_i and are given by Equations (A12) – (A15) in Appendix A. a_i and γ_i are the azimuthal angle and the incident angle at ΔA_i. θ_i is the angle between the vertical axis and the line joining the antenna and ΔA_i. β_i is the angle between ΔA_i and the horizontal plane. θ and a have the same meaning as before. The measured antenna patterns for both horizontal and vertical polarizations were found to be rather similar and were assumed to be the same for simplicity. The summations in Equations (3) and (4) are made over the footprint of the antenna.

The numerical calculations of $T_{BH}(\theta, \alpha)$ and $T_{BV}(\theta, \alpha)$ were carried out with $\Delta X_i = \Delta Y_i = 5$ cm. The height of the antenna was taken to be 14 m above the surface. The small-scale RMS height variations of the field were estimated from the surface profiles taken at both ridges and furrows. The average values are found to be ~2.78 cm for ridges and ~1.72 cm for furrows, which fall between the smooth and the medium rough surfaces according to the criteria of Newton (4) and Choudhury et al. (8). Thus, h was chosen to be ~0.30 in the calculations of $T_{BH}(\gamma_i)$ and $T_{BV}(\gamma_i)$. The soil temperature and moisture profiles used in the calculations were the smoothed results of the actually measured values taken within ~ ±1 hour of the radiometric measurements at the depths of 0-1 cm, 1-2 cm, 2-5 cm, 5-9 cm, and 9-15 cm. For depth >15 cm, both soil temperature and moisture content were assumed to be constant and equal to the values measured at 9-15 cm. The calculations were made to a depth of ~100 cm which is sufficient considering the sampling depth of ~5-10 cm at 21 cm wavelength (8). The relationship between the dielectric constant and the moisture content for the Miller Clay was obtained from the measurements of Newton and McClellan (14).

The results of the calculations for the measurements on July 16 at $\alpha = 0°$ and $\alpha = 90°$ are shown by the solid smooth curves in Figure 9, a and b. The measured data are also included in the figure for comparison. It is clear that the results of the calculations including the effect of the sinusoidal variations of the row structure gave a good agreement to the observed data. At $\theta = 0°$, the observed differences between $T_{BH}(0°, 0°)$ and $T_{BV}(0°, 0°)$ and between $T_{BH}(0°, 90°)$ and $T_{BV}(0°, 90°)$ are clearly displayed by the results of the numerical calculations.

Figure 10 shows both the observed and calculated variations of $T_{NH}(0°, 0°) - T_{NV}(0°, 0°)$ and $T_{NV}(0°, 90°) - T_{NH}(0°, 90°)$ as a function of soil moisture content. All the calculations were made with the same h value and with both soil temperature and moisture profiles taken within ~ ±1 hour of radiometric measurements. For a few cases in which the ground truth data and the radiometric measurements did not coincide, the soil temperature and moisture profiles averaged over a two-hour period closest to the time of the radiometric measurements were used. It is noted from the figure that two features from the calculated results are in accordance with the observations. First, the normalized antenna temperature differences are present over the moisture range of ~10 - 30%. Secondly, the magnitude of the differences decreases with soil moisture content. However, the calculated dependence of the antenna temperature difference on the moisture content is not as strong

compared to the observed results. At high moisture content the calculated antenna temperature differences are less than the observed ones. At low moisture content, the calculations give higher values than the observed ones.

5. DISCUSSION

The simple composite surface roughness model described in the previous section accounts for the most features exhibited by the measured data, although the magnitude of these features is not always predicted accurately. This is evident in the systematic difference between the calculated and the observed values of $T_{NH}(0°, 0°) - T_{NV}(0°, 0°)$ and $T_{NV}(0°, 90°) - T_{NH}(0°, 90°)$ shown in Figure 10. Contributions to the discrepancies between the calculated and the observed results may come from many factors. One of these factors could be the very different characteristics of soils at the ridges and the furrows of the field. A close examination of the data reported by Newton and Tesch (10) indicates that the moisture contents measured at the ridges are generally less than those measured at the furrows. The average bulk density of the dry soil at the ridges was found to be less than that at the furrows. The small scale RMS height variations measured at the ridges were found to be larger than those measured at the furrows. As a consequence, the contributions to the observed antenna temperature from the ridge portion and from the furrow portion of the field could be very different. The actual variations of the moisture, temperature, and density profiles, as well as the parameter h from the ridge to the furrow may have significant bearing on the brightness temperature calculation which the simple model presented here is not capable of handling.

Improved correspondence between the model predictions and the measurements should be obtained with a better estimate of the roughness factor h given by Eq. (2). The assumption that h is independent of local incident angle γ_i was based on the first order estimate of the flat field measurements over a limited range of γ_i, 0°-50°, (12). In the numerical calculation this independence was assumed for a range of γ_i over 0°-90°. A limited measurement on the RMS surface roughness effect by Hancock (15), however, implies that the roughness parameter h may depend on γ_i. Furthermore, the difference in the RMS height variations in the ridges and furrows of the field suggests that a constant h adopted in the present calculation may not be strictly valid. With different form for $r_p(\gamma_i)$, the calculated $T_{BH}(\theta, a)$ and $T_{BV}(\theta, a)$ could be quite different from the ones shown in Figure 9, a and b, and Figure 10.

Other factors like the general slope of the field, skewness of the rows, and the uncertainties in the radiometric measurements and ground truth data take could all affect the observed results and are difficult to take into account in the calculations. However, the most important is the fact that the row structure in the microwave emission from an agricultural field can be understood in terms of the simple model presented above.

6. CONCLUSION

It has been shown that the presence of the periodic row structure could have an appreciable effect on the microwave emission from an agricultural field. This effect should be realized and, whenever possible, corrected to improve the precision of microwave remote sensing of surface soil moisture content. The analyses on the observational results and the calculations based on the simple composite surface roughness model suggest that:

- At $\theta = 0°$ and azimuthal angle (measured from the row direction) $a \neq 45°$, $T_{BH}(0°, a)$ and $T_{BV}(0°, a)$ are not equal. For $0° \leq a < 45°$, $T_{BH}(0°, a) > T_{BV}(0°, a)$, and for $45° < a \leq 90°$, $T_{BV}(0°, a) > T_{BH}(0°, a)$. The absolute values of $T_{BV}(0°, a) - T_{BH}(0°, a)$ decreases as a approaches 45°.
- The absolute values of $T_{BV}(0°, a) - T_{BH}(0°, a)$ are observed to decrease with soil moisture content.
- When properly normalized to soil temperature, it is observed that $T_{BV}(0°, 90°) \simeq T_{BH}(0°, 0°)$ and $T_{BV}(0°, 0°) \simeq T_{BH}(0°, 90°)$.
- A simple composite surface roughness model consisting of the small-scale random surface roughness superimposed on the large-scale sinusoidal surface variations of the row structure seems able to account for the gross observed features summarized above.

APPENDIX A

Assuming that the large-scale surface variations of the field with regularly spaced rows as shown in Figure 8 can be described by a sinusoidal wave

$$Z = \left(1 + \left(\frac{2\pi Y}{95}\right)\right) X10 \tag{A1}$$

where the measured height of ~20 cm and period of ~95 cm of the rows are explicitly entered in the equation. The angle β_i between the surface element ΔA_i and the horizontal plane is given by

$$\beta_i = \tan^{-1}\left(-\frac{20\pi}{95}\sin\left(\frac{2\pi Y}{95}\right)\right) \tag{A2}$$

The unit vectors $\hat{n}_i$ and $\hat{k}_i$ for the normal to ΔA_i and for the line of the wave propagation from ΔA_i to observation point P can be expressed as

$$\hat{n}_i = (0, -\sin\beta_i, \cos\beta_i) \tag{A3}$$

$$\hat{k}_i = (-\sin\theta_i\cos a_i, -\sin\theta_i\sin a_i, \cos\theta_i) \tag{A4}$$

where θ_i is the angle between $\hat{k}_i$ and the vertical axis, and a_i is the azimuthal angle at ΔA_i measured from the X-axis (parallel to row direction). The incident angle γ_i local to ΔA_i is obtained by the dot product of Eqs. (A3) and (A4):

$$\cos\gamma_i = \cos\beta_i\cos\theta_i + \sin\beta_i\sin\theta_i\sin a_i \tag{A5}$$

The unit vectors $\hat{e}_H$ and $\hat{e}_V$ for the horizontally and the vertically polarized electric fields $\bar{E}_H(\gamma_i)$ and $\bar{E}_V(\gamma_i)$ are easily derived from Eqs. (A3) and (A4) and are given by

$$\hat{e}_H = \frac{1}{\sin\gamma_i}(-\sin\beta_i\cos\theta_i + \cos\beta_i\sin\theta_i\sin a_i, -\cos\beta_i\sin\theta_i\cos a_i, -\sin\beta_i\sin\theta_i\cos a_i) \tag{A6}$$

$$\hat{e}_V = \frac{1}{\sin\gamma_i}(\sin\theta_i\cos a_i\cos\gamma_i, -\sin\beta_i + \sin\theta_i\sin a_i\cos\gamma_i, \cos\beta_i - \cos\theta_i\cos\gamma_i) \tag{A7}$$

The polarizations of a radiometer antenna are generally different from the directions of $\hat{e}_H$ and $\hat{e}_V$. For the given incident angle θ and the azimuthal angle a, the unit vectors of the antenna polarizations are:

$$\hat{a}_H = (\sin\alpha, -\cos\alpha, 0) \tag{A8}$$

$$\hat{a}_V = (\cos\theta\cos\alpha, \cos\theta\sin\alpha, \sin\theta) \tag{A9}$$

Only the components of the radiation fields along the directions of antenna polarizations are observed by the radiometer. Thus the electric fields along the horizontal and vertical polarizations of the antenna, E_{aH} and E_{aV}, are given by

$$E_{aH} = \hat{a}_H \cdot (\mathcal{E}_H(\gamma_i)\hat{e}_H + \mathcal{E}_V(\gamma_i)\hat{e}_V) \tag{A10}$$

$$= \frac{\mathcal{E}_H(\gamma_i)A + \mathcal{E}_V(\gamma_i)B}{\sin\gamma_i}$$

$$E_{aV} = \hat{a}_V \cdot (\mathcal{E}_H(\gamma_i)\hat{e}_H + \mathcal{E}_V(\gamma_i)\hat{e}_V) \tag{A11}$$

$$= \frac{\mathcal{E}_H(\gamma_i)C + \mathcal{E}_V(\gamma_i)D}{\sin\gamma_i}$$

where

$$A = -\sin\alpha\sin\beta_i\cos\theta_i + \cos\beta_i\sin\theta_i\cos(\alpha_i - \alpha) \tag{A12}$$

$$B = -\sin\theta_i\sin(\alpha_i - \alpha)\cos\gamma_i + \cos\alpha\sin\beta_i \tag{A13}$$

$$C = -\cos\theta\cos\alpha\sin\beta_i\cos\theta_i + \cos\theta\cos\beta_i\sin\theta_i\sin(\alpha_i - \alpha) \tag{A14}$$

$$-\sin\theta\sin\beta_i\sin\theta_i\cos\alpha_i$$

$$D = -\cos\theta\sin\alpha\sin\beta_i + \sin\theta\cos\beta_i - \sin\theta\cos\theta_i\cos\gamma_i \tag{A15}$$

$$+ \cos\theta\sin\theta_i\cos(\alpha_i - \alpha)\cos\gamma_i$$

Since the brightness temperature is proportional to the square of the electric field, the observed $T^i_{BH}(\theta, \alpha)$ and $T^i_{BV}(\theta, \alpha)$ from ΔA_i by the radiometer are

$$T^i_{BH}(\theta, \alpha) = \frac{T^i_{BH}(\gamma_i)A^2 + T^i_{BV}(\gamma_i)B^2}{\sin^2\gamma_i} \tag{A16}$$

$$T^i_{BV}(\theta, \alpha) = \frac{T^i_{BH}(\gamma_i)C^2 + T^i_{BV}(\gamma_i)D^2}{\sin^2\gamma_i} \tag{A17}$$

The cross terms involving $\mathcal{E}_H(\gamma)\mathcal{E}_V(\gamma)AB$ and $\mathcal{E}_H(\gamma)\mathcal{E}_V(\gamma)CD$ drop out on the average since $\mathcal{E}_H(\gamma)$ and $\mathcal{E}_V(\gamma_i)$ are not correlated (16). Summing over the footprint of the radiometer and taking into account the antenna gain and solid angle factor, the observed brightness temperatures $T_{BH}(\theta, \alpha)$ and $T_{BV}(\theta, \alpha)$ are obtained and given by Equations (3) and (4).

The brightness temperatures $T^i_{BH}(\gamma_i)$ and $T^i_{BV}(\gamma_i)$ from the surface element ΔA_i can be calculated by the one-parameter small-scale surface roughness model of Choudhury et al. (8).

REFERENCES

[1] Schmugge, T., P. Gloerson, T. Wilheit, and F. Geiger, "Remote Sensing of Soil Moisture With Microwave Radiometers," J. Geophys. Res., 79, p. 317, 1974.

[2] Njoku, E. G. and J. A. Kong, "Theory for Passive Microwave Remote Sensing of Near Surface Soil Moisture," J. Geophys. Res., 82, pp. 3108-3117, 1977.

[3] Schmugge, T. J., T. T. Wilheit, W. Webster, and P. Gloersen, "Remote Sensing of Soil Moisture With Microwave Radiometers II," NASA Technical Note, TND-8321, 1976.

[4] Newton, R. W., "Microwave Remote Sensing and its Application to Soil Moisture Detection," Technical Report RCS-81, Remote Sensing Center, Texas A&M University, College Station, Texas, 1977.

[5] Ludien, J. R., "Terrain Analysis by Electromagnetic Means, U.S. Army Waterways Experiment Station," Technical Report No. 3-693, Report 5, 1971.

[6] Wang, J. R., and T. J. Schmugge, "An Empirical Model for the Complex Dielectric Permittivity of Soils as a Function of Water Content," NASA TM-79659, 1978.

[7] Schmugge, T. J., B. J. Blanchard, W. J. Burke, J. F. Paris, and J. R. Wang, "Results of Soil Moisture Flights During April 1974," NASA Technical Note, TND-8199, 1976.

[8] Choudhury, B. J., T. J. Schmugge, R. W. Newton and A. Chang, "Effect of Surface Roughness on the Microwave Emission from Soils," NASA TM 79606, 1978.

[9] Sibley, T. G., "Microwave Emission and Scattering from Vegetated Terrain," Technical Report RSC - 44, Remote Sensing Center, Texas A&M University, College Station, Texas, 1973.

[10] Newton, R. W., and E. A. Tesch, "Joint Soil Moisture Experiment Ground Based Measurements at Texas A&M University, July 13 - July 25, 1975," Technical Report RSC-71, Remote Sensing Center, Texas A&M University, College Station, Texas, 1976.

[11] Rose, C. W., "Water Transport in Soil With a Daily Temperature Wave: I. Theory and Experiment," Aust. J. Soil Res., 6, pp. 31-34, 1968.

[12] Newton, R. W., "Joint Soil Moisture Experiment at Texas A&M University, June 26 - July 21, 1974," Technical Report RSC-65, Remote Sensing Center, Texas A&M University, College Station, Texas, 1975.

[13] Wilheit, T. T., "Radiative Transfer in a Plane Stratified Dielectric," IEEE Trans. Geosci. Electronics, Vol. GE-16 (2), pp. 138-143, 1978.

[14] Newton, R. W., and W. R. McClellan III, "Permittivity Measurements of Soils at L-Band," Technical Report RSC-58, Remote Sensing Center, Texas A&M University, College Station, Texas, 1975.

[15] Hancock, G. D., "Broad Spectrum Microwave Measurements of Rough Discontinuous Surfaces for the Determination of Moisture Content," Dept. of Electrical Engineering, University of Arkansas, Arkansas 72701, 1976.

[16] Grody, N. C., "Antenna Temperature for a Scanning Microwave Radiometer," IEEE Trans. Antenna Propagat., Vol. AP-23, No. 1, pp. 141-144, 1975.

Figure Captions

Figure 1. The measured L-band brightness temperatures on July 16, 1975 as a function of incident angle θ, with azimuthal angle α of 0°, 30°, 60°, and 90°. The polarizations of the brightness temperatures are indicated by H (horizontal) and V (vertical).

Figure 2. The measured L-band brightness temperatures on July 25, 1975 as a function of incident angle θ, with azimuthal angle α of 0°, 45° and 90°. The polarizations of the brightness temperatures are indicated by H (horizontal) and V (vertical).

Figure 3. The measured X-band brightness temperatures on July 16, 1975 as a function of incident angle θ, with azimuthal angle α of 0°, 30°, 60°, and 90°. The polarizations of the brightness temperatures are indicated by H (horizontal) and V (vertical).

Figure 4. The difference between the horizontally and vertically polarized X-band brightness temperatures measured at nadir incidence plotted as a function of azimuthal angle α.

Figure 5. Antenna measurement angular response and polarization referred to the plane of incidence defined by the look direction and the nadir vector.

Figure 6. The time history of the soil moisture content, normalized brightness temperatures and their differences for the entire radiometric measurements in July 1975.

Figure 7. The regression plot of the normalized brightness temperatures at nadir incidence and the soil moisture contents. The equivalences between $T_{NV}(0°, 0°)$ and $T_{NH}(0°, 90°)$ and between $T_{NH}(0°, 0°)$ and $T_{NV}(0°, 90°)$ are clearly shown by the plot.

Figure 8. A sketch showing the sinusoidal nature of the row structure used in the simple composite surface roughness model calculations.

Figure 9. A comparison of the measured and calculated brightness temperatures as a function of incident angle for measurements on July 16, 1975. (a): $\alpha = 0°$, (b): $\alpha = 90°$.

Figure 10. The variations of the measured and the calculated normalized brightness temperature differences as a function of soil moisture content.

Table 1
The Measured Brightness Temperature at $\theta = 0°$ and $\alpha = 0°$, 90°, and the Associated Soil Temperature and Moisture Content at Top 2-cm Layer

Date	Time	Polarization	Azimuth Angle Degrees	Antenna Temperature °K	Soil Temperature °K (0-2 cm)	Moisture Content (0-2 cm) % Dry Weight	Normalized Antenna Temperature
July 16	7:55 - 9:27	H V	90° 90°	219.31 236.88	299.0	29.84	0.733 0.791
	12:12 - 13:50	H V	0° 0°	252.71 239.27	304.5	26.49	0.831 0.786
July 17	7:46 - 9:16	H V	0° 0°	256.57 244.56	297.4	22.59	0.862 0.822
	11:20 - 12:36	H V	90° 90°	256.99 266.41	305.6	20.88	0.841 0.872
July 18	15:17 - 17:05	H V	90° 90°	256.49 267.97	307.1	21.00	0.835 0.872
	19:13 - 20:41	H V	0° 0°	268.18 258.18	305.3	17.69	0.879 0.846
July 20	15:02 - 16:31	H V	90° 90°	253.10 264.06	310.4	17.73	0.815 0.850
	16:56 - 18:17	H V	0° 0°	262.77 251.60	308.4	17.30	0.853 0.816
July 21	7:27 - 8:55	H V	90° 90°	251.54 261.53	301.7	18.55	0.833 0.866
	11:05 - 12:16	H V	0° 0°	267.94 258.27	307.9	17.63	0.870 0.840
July 22	7:08 - 8:15	H V	0° 0°	271.25 262.78	298.9	16.31	0.908 0.880
	10:35 - 11:37	H V	90° 90°	272.28 280.27	305.5	15.37	0.893 0.918
July 24	7:48- 8:48	H V	90° 90°	267.91 275.26	300.6	13.71	0.891 0.915
	14:15 - 15:32	H V	0° 0°	288.95 282.90	305.9	12.50	0.946 0.925
July 25	8:45 - 9:52	H V	90° 90°	272.00 278.97	305.3	11.99	0.891 0.914
	12:03 - 13:02	H V	0° 0°	287.12 281.34	307.4	11.07	0.935 0.916

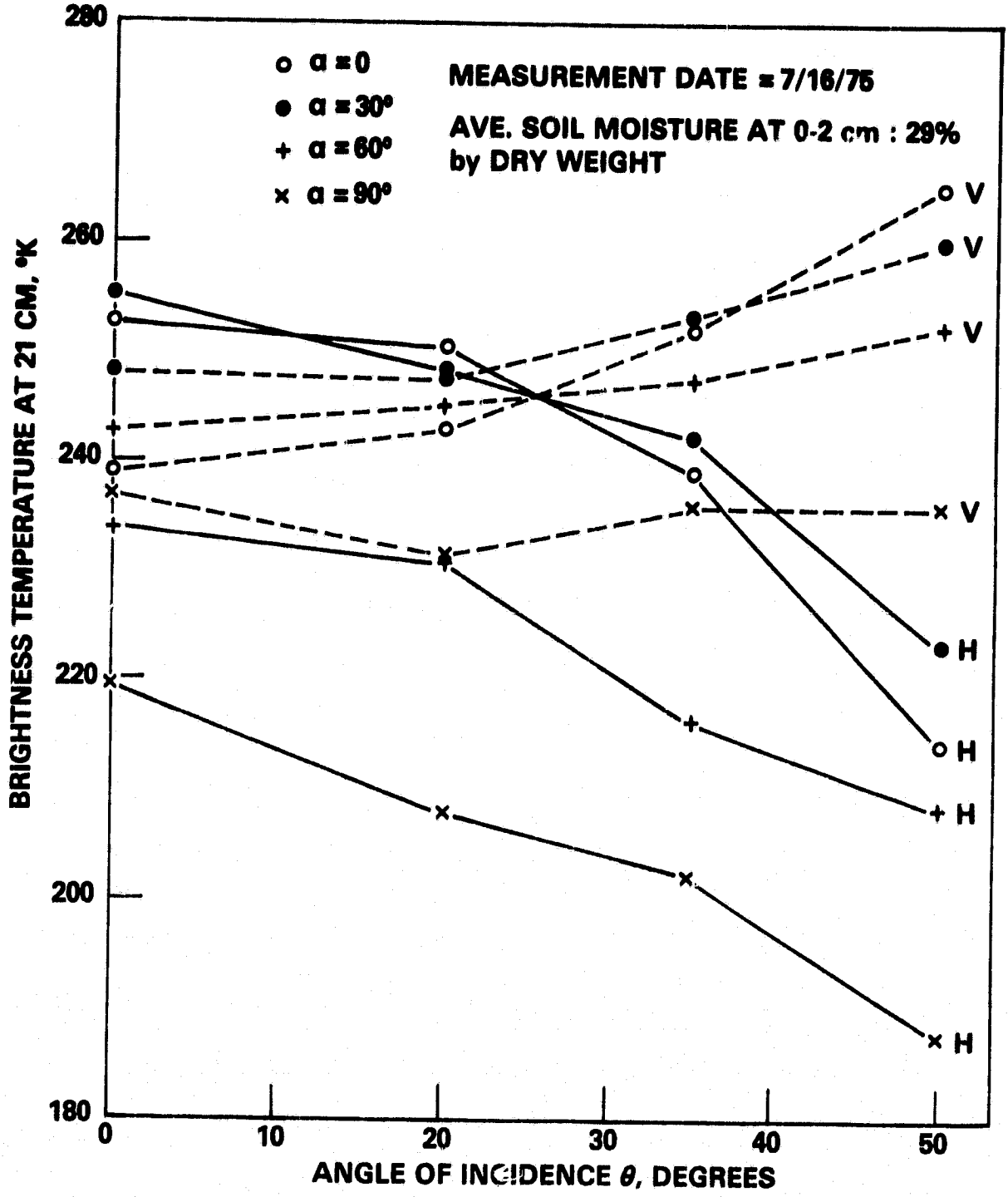

Figure 1. The measured L-band brightness temperatures on July 16, 1975 as a function of incident angle θ, with azimuthal angle α of 0°, 30°, 60°, and 90°. The polarizations of the brightness temperatures are indicated by H (horizontal) and V (vertical).

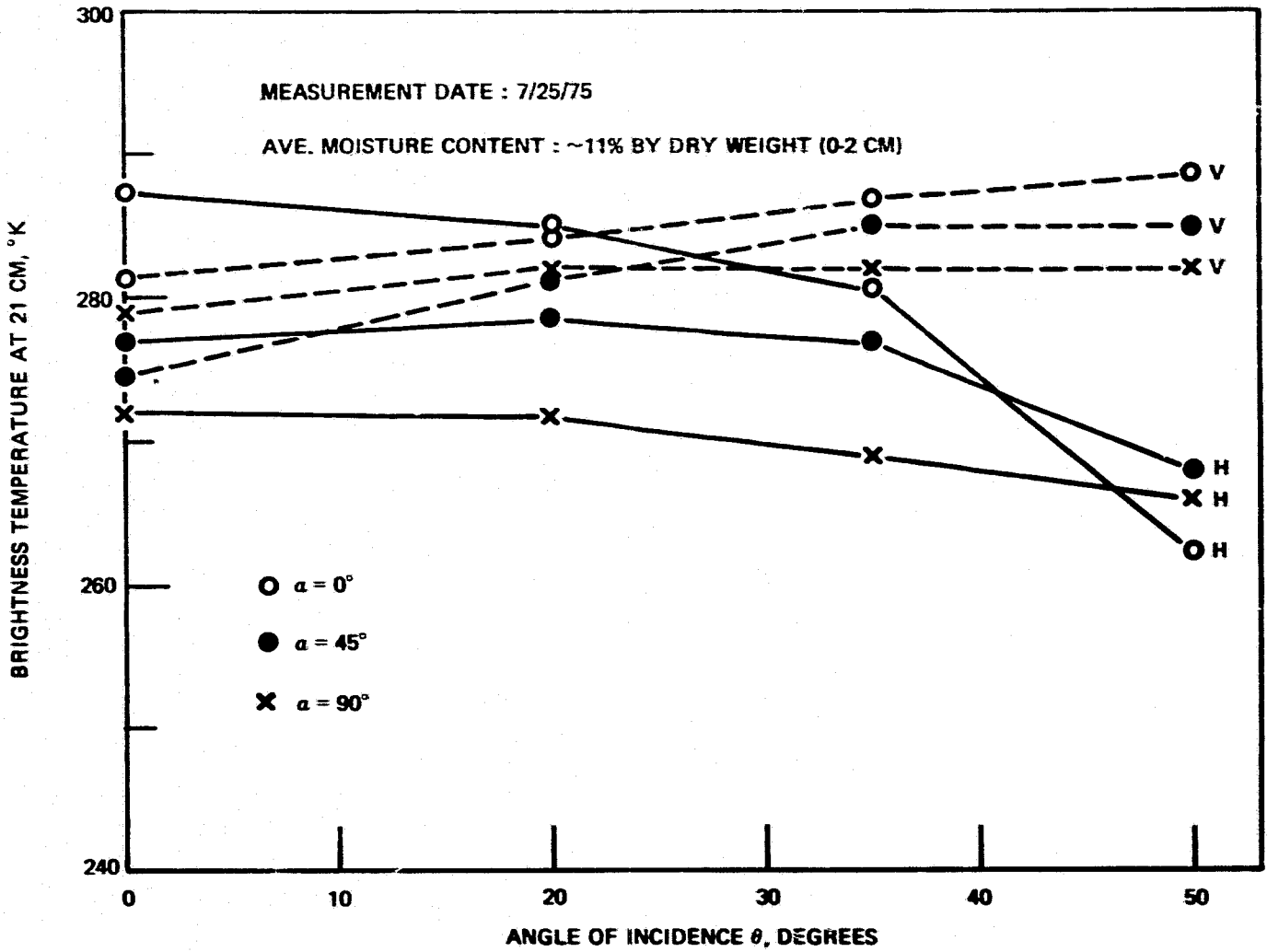

Figure 2. The measured L-band brightness temperatures on July 25, 1975 as a function of incident angle θ, with azimuthal angle α of 0°, 45° and 90°. The polarizations of the brightness temperatures are indicated by H (horizontal) and V (vertical).

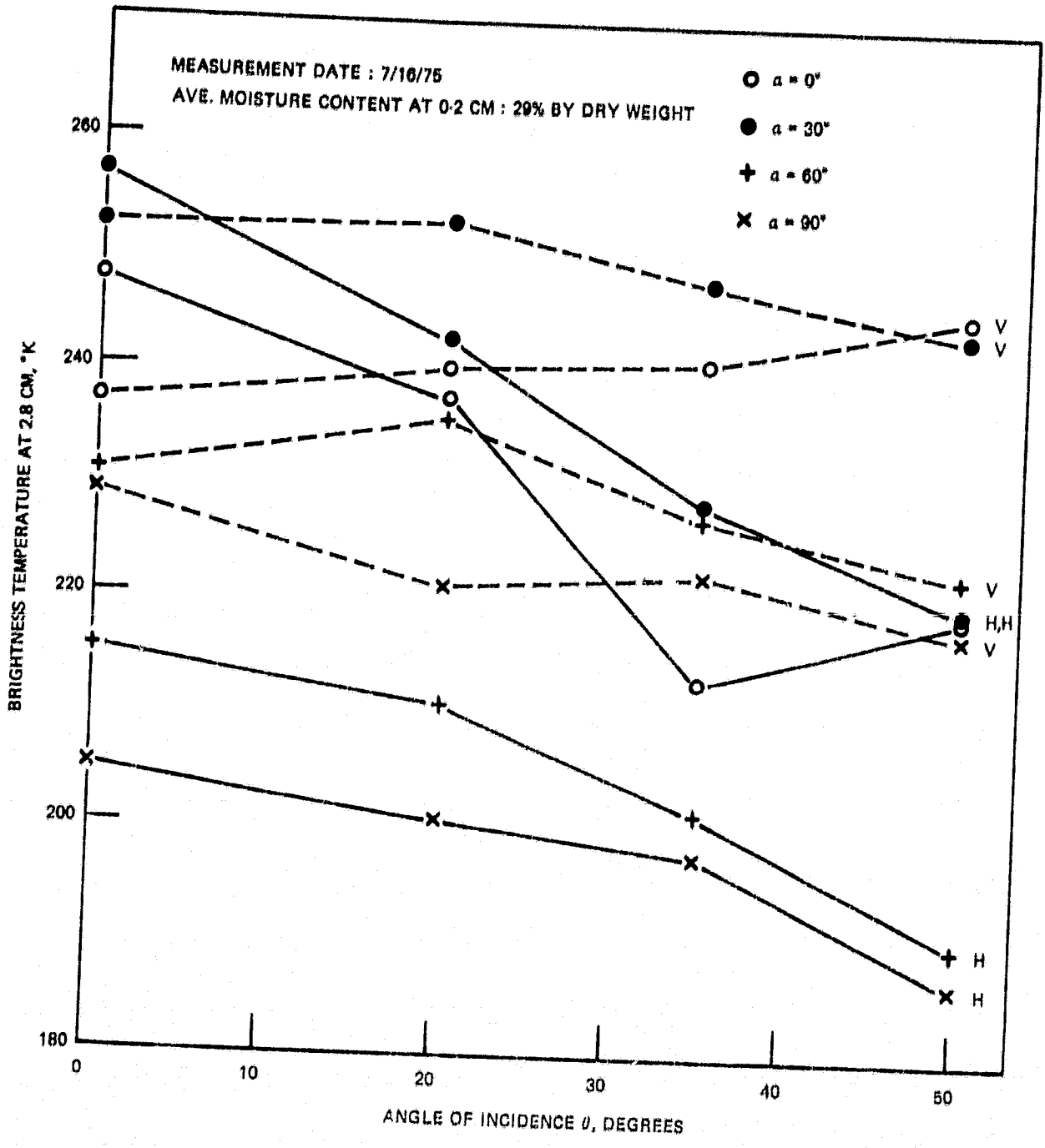

Figure 3. The measured X-band brightness temperatures on July 16, 1975 as a function of incident angle θ, with azimuthal angle α of 0°, 30°, 60°, and 90°. The polarizations of the brightness temperatures are indicated by H (horizontal) and V (vertical).

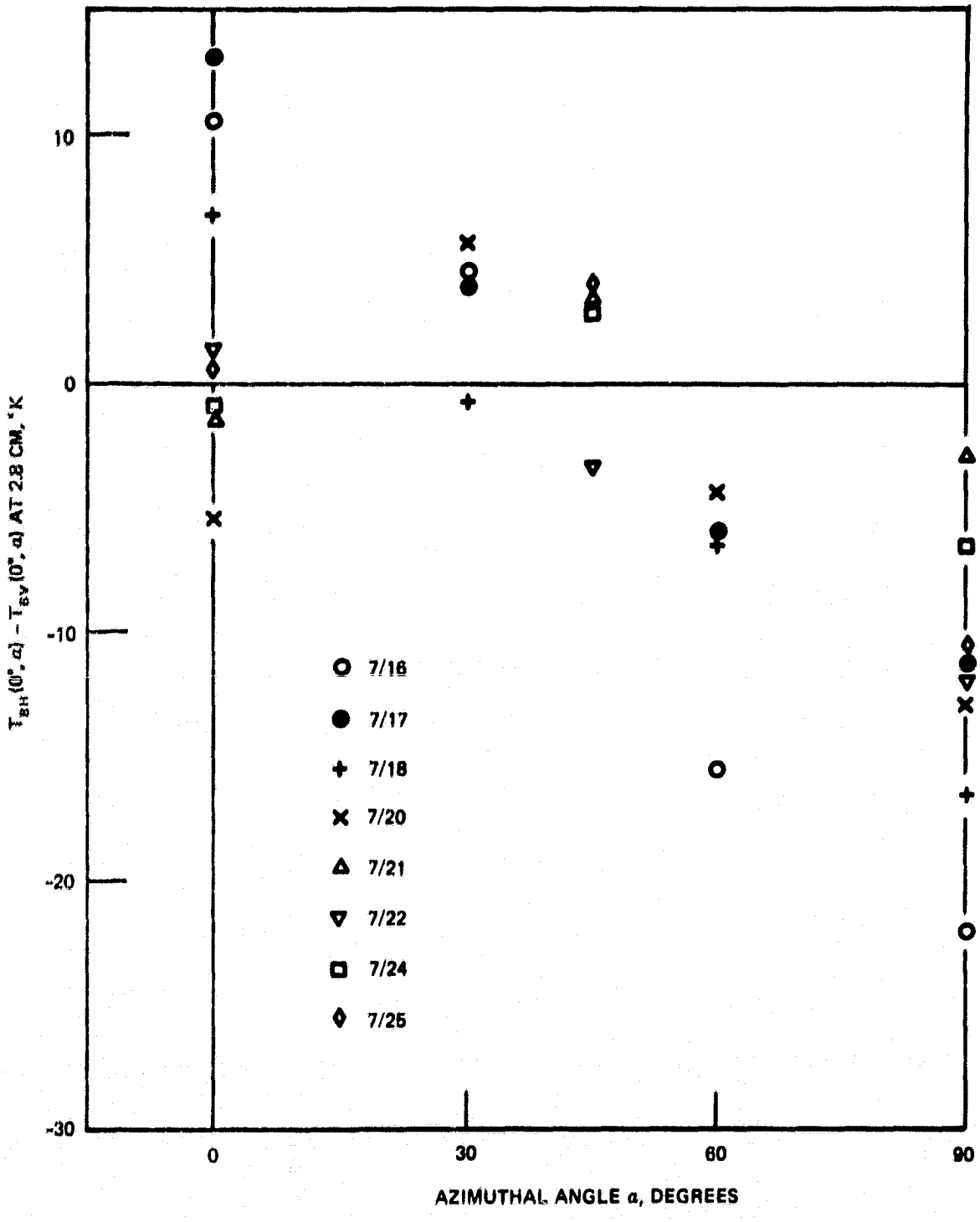

Figure 4. The difference between the horizontally and vertically polarized X-band brightness temperatures measured at nadir incidence plotted as a function of azimuthal angle α.

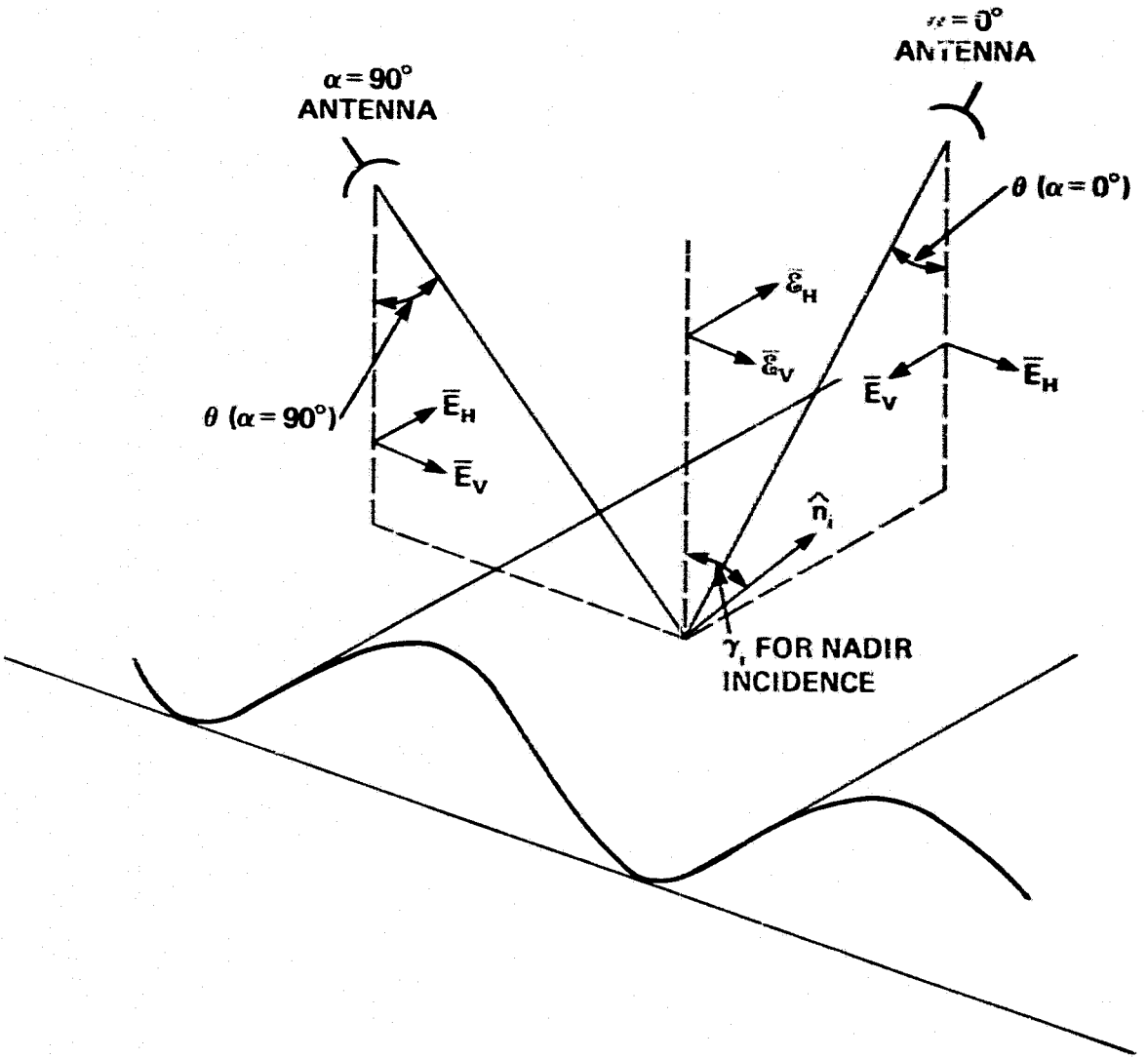

Figure 5. Antenna measurement angular response and polarization referred to the plane of incidence defined by the look direction and the nadir vector.

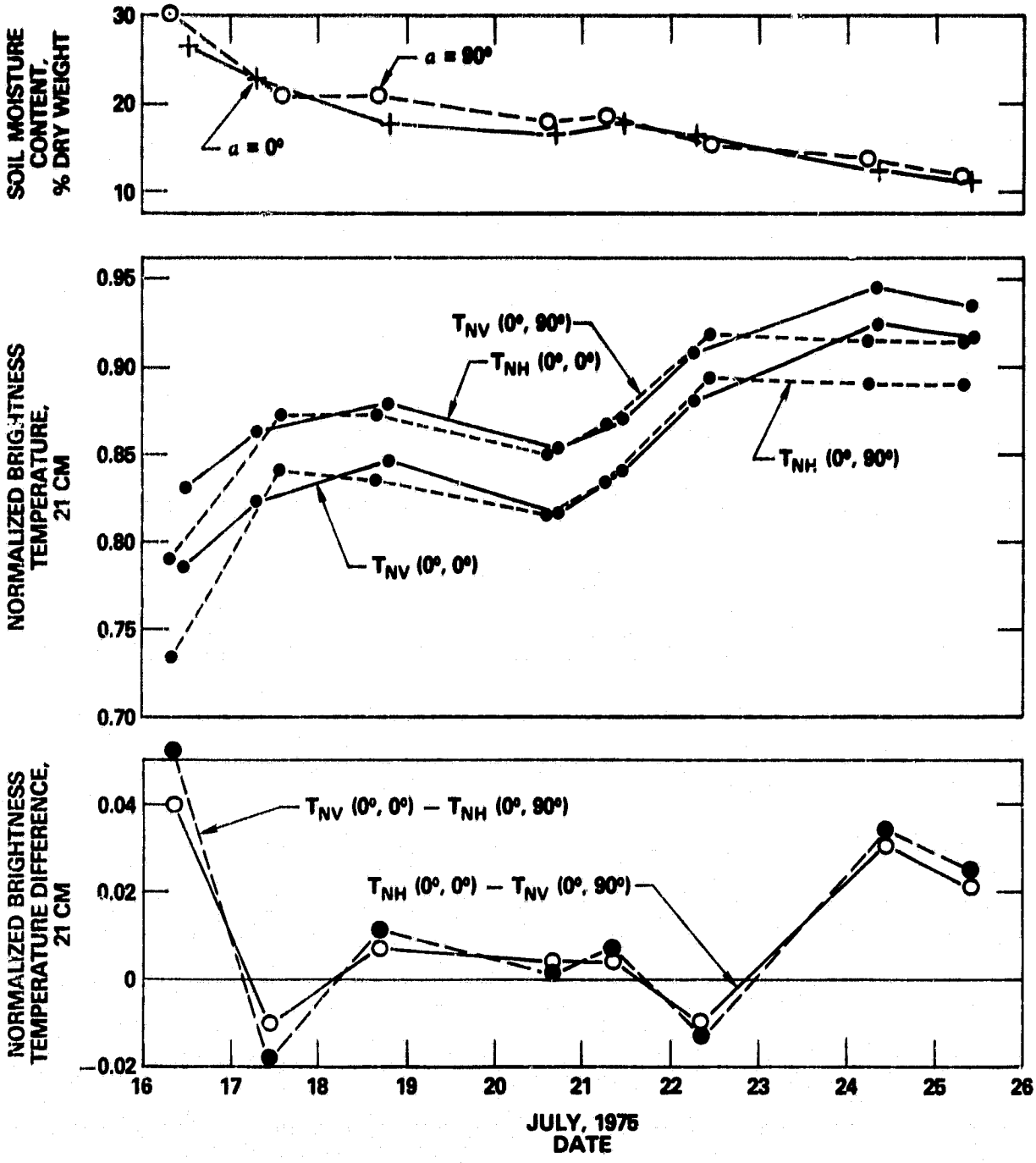

Figure 6. The time history of the soil moisture content, normalized brightness temperatures and their differences for the entire radiometric measurements in July 1975.

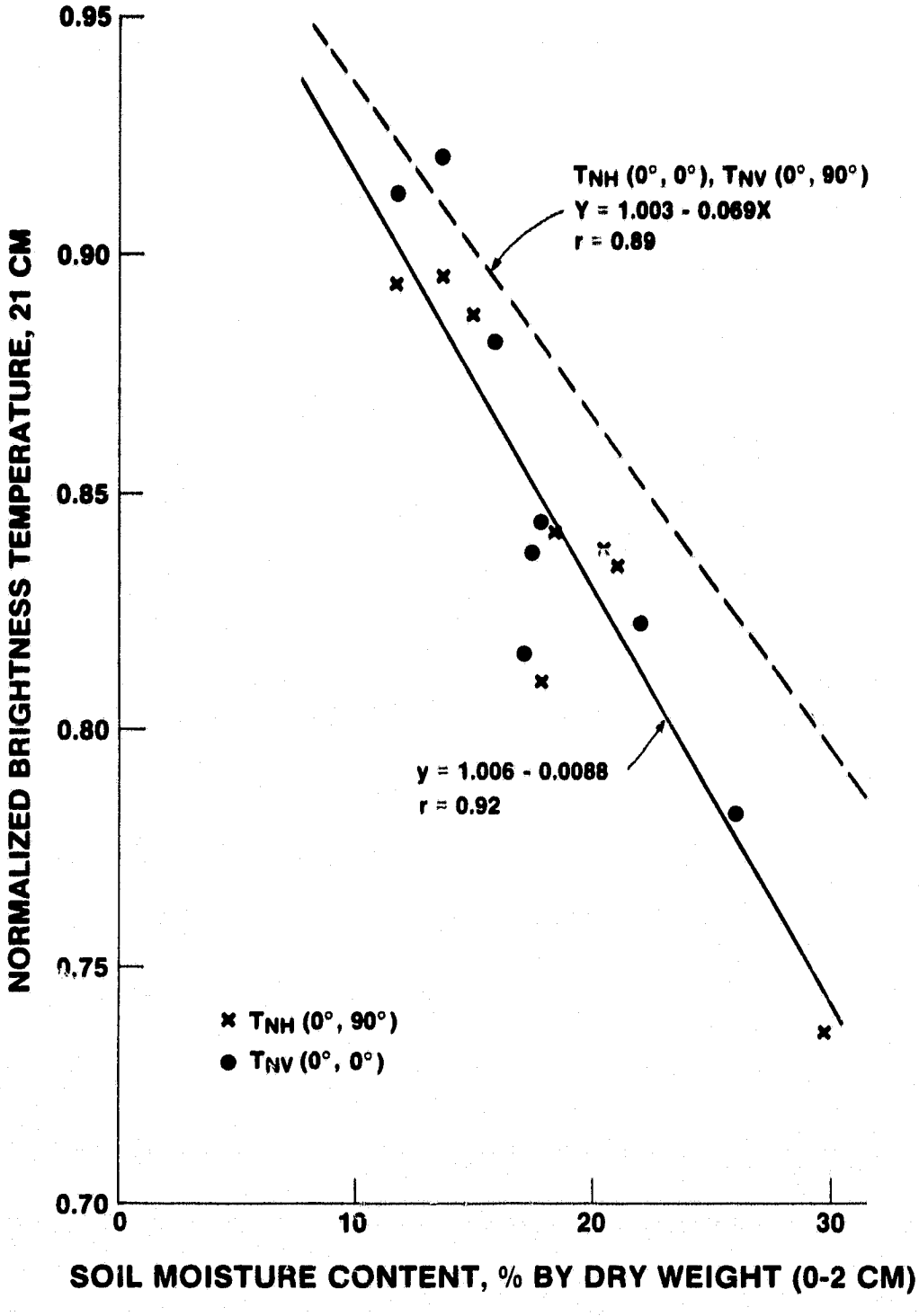

Figure 7. The regression plot of the normalized brightness temperatures at nadir incidence and the soil moisture contents. The equivalences between $T_{NV}(0°, 0°)$ and $T_{NH}(0°, 90°)$ and between $T_{NH}(0°, 0°)$ and $T_{NV}(0°, 90°)$ are clearly shown by the plot.

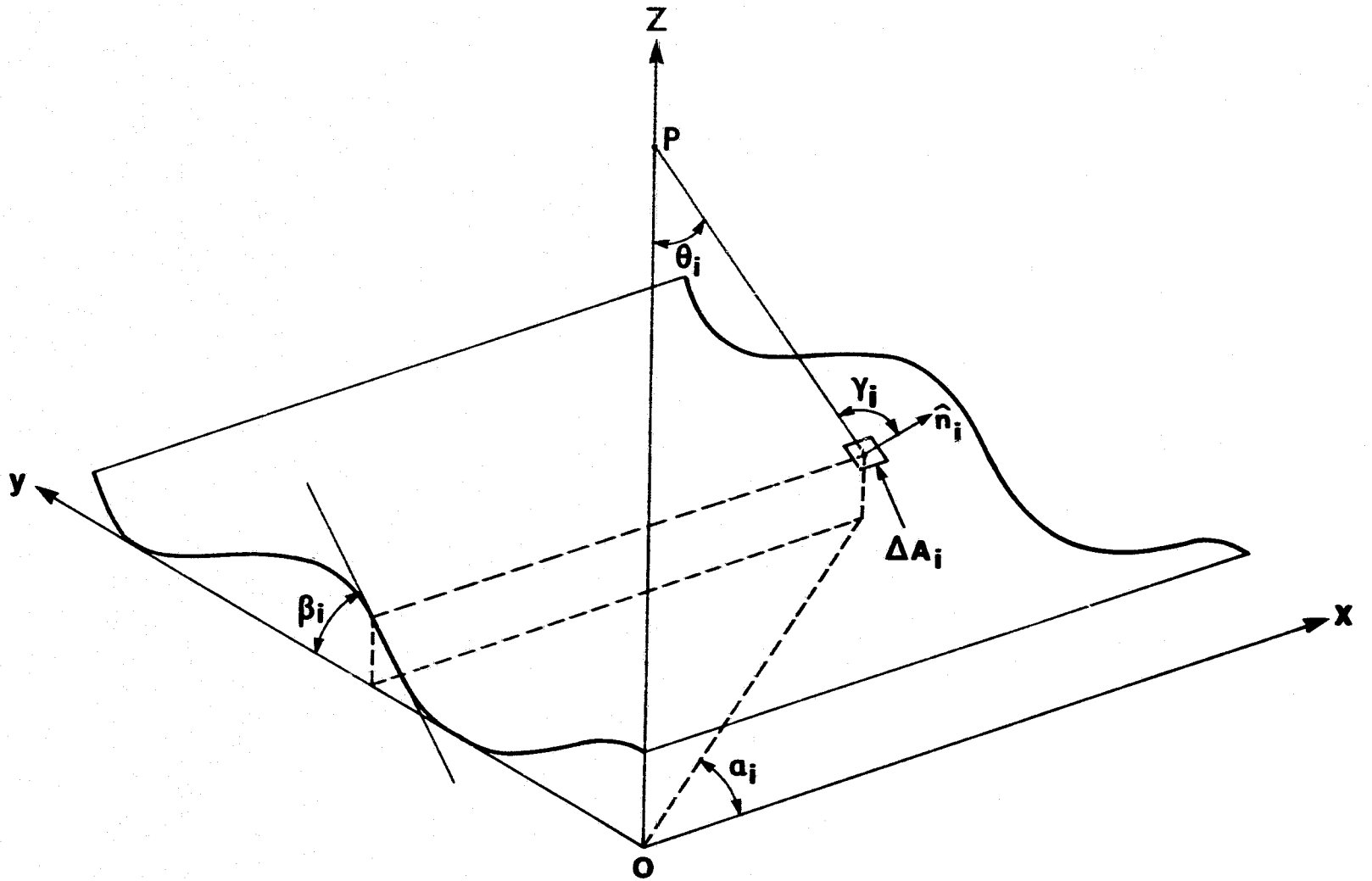

Figure 8. A sketch showing the sinusoidal nature of the row structure used in the simple composite surface roughness model calculations.

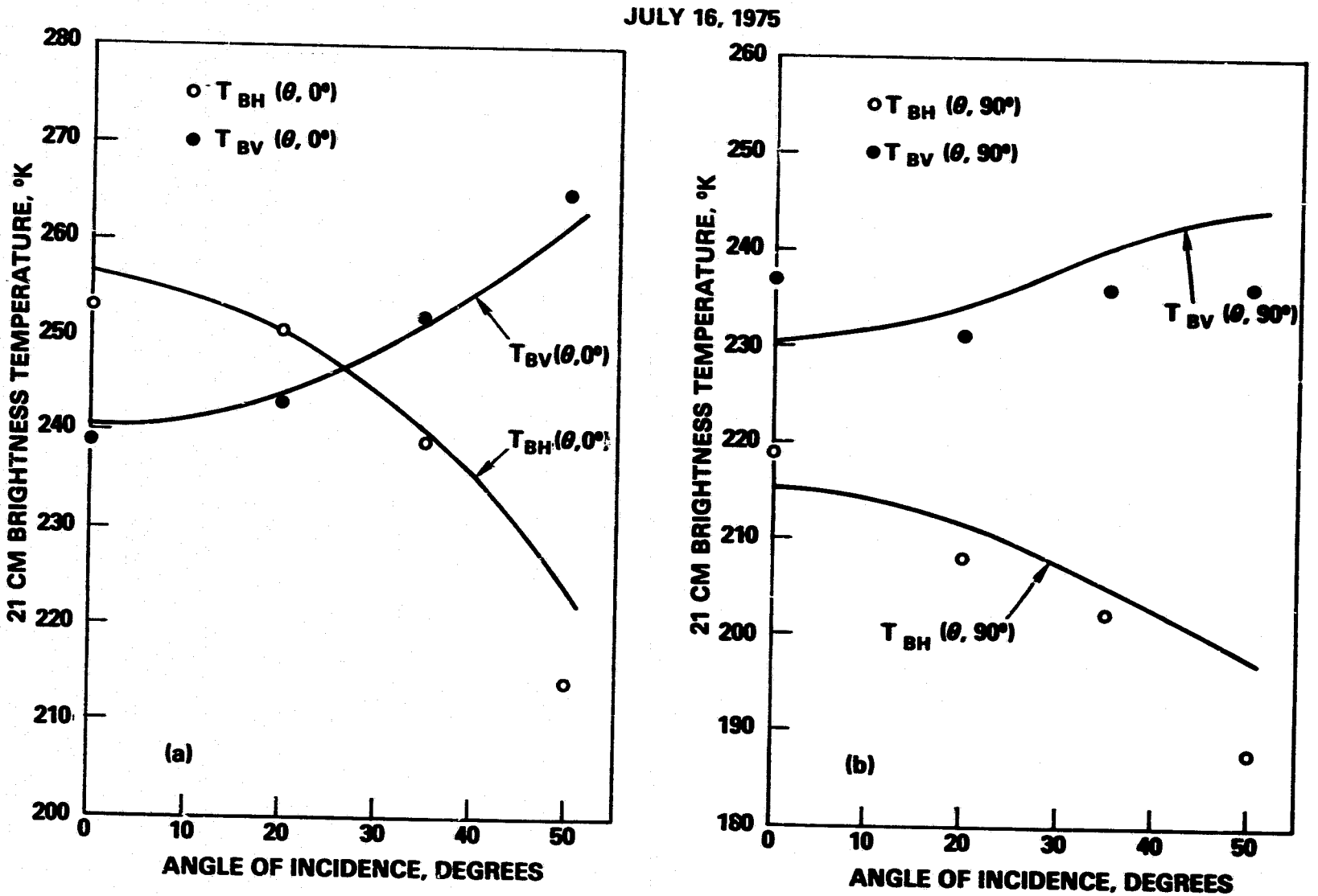

Figure 9. A comparison of the measured and calculated brightness temperatures as a function of incident angle for measurements on July 16, 1975. (a): $\alpha = 0°$, (b): $\alpha = 90°$.

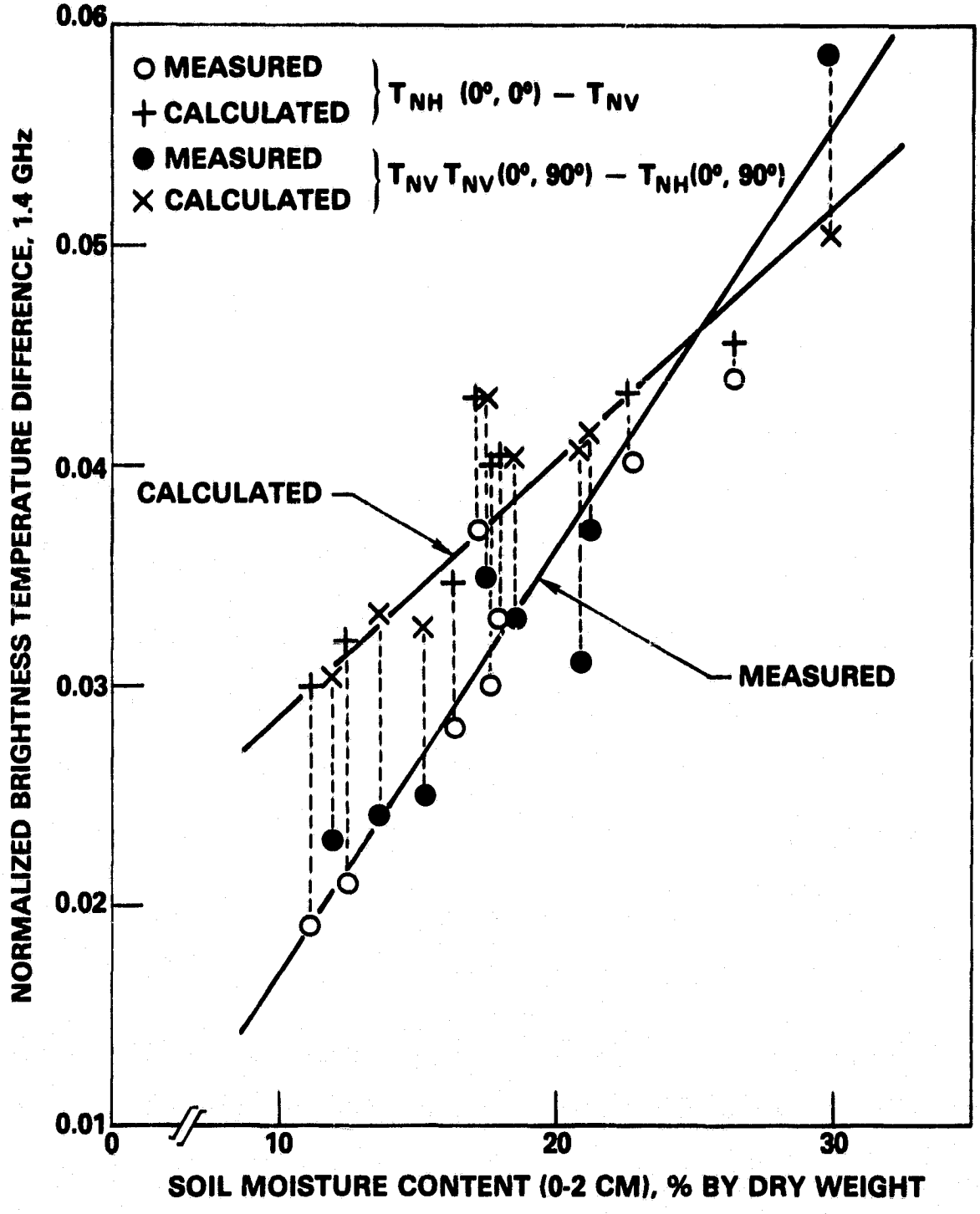

Figure 10. The variations of the measured and the calculated normalized brightness temperature differences as a function of soil moisture content.

BIBLIOGRAPHIC DATA SHEET

1. Report No.	2. Government Accession No.	3. Recipient's Catalog No.
4. Title and Subtitle Passive Microwave Remote Sensing of Soil Moisture: The Effect of Tilled Row Structure		5. Report Date June 1979 6. Performing Organization Code
7. Author(s) J. R. Wang, R. W. Newton, and J. W. Rouse		8. Performing Organization Report No.
9. Performing Organization Name and Address Goddard Space Flight Center Greenbelt, Maryland 20771		10. Work Unit No. 11. Contract or Grant No. 13. Type of Report and Period Covered
12. Sponsoring Agency Name and Address		14. Sponsoring Agency Code
15. Supplementary Notes		

16. Abstract

The tilled row structure is known to be one of the important factors affecting the observations of the microwave emission from a natural surface. Measurements of this effect were carried out with both L- and X-band radiometers mounted on a mobile truck on a bare 40 m x 45 m row tilled field. The soil moisture content during the measurements ranged from ~10% to ~30% by dry weight. The results of these measurements showed that the variations of the antenna temperatures with incident angle θ changed with the azimuthal angle a measured from the row direction. In particular, at $\theta = 0°$ and $a \neq 45°$, the observed horizontally and vertically polarized antenna temperatures, $T_{BH}(\theta, a)$ and $T_{BV}(\theta, a)$, were not equal. In general, $T_{BH}(0°, a) > T_{BV}(0°, a)$ when $0° \leq a < 45°$ and $T_{BH}(0°, a) < T_{BV}(0°, a)$ when $45° < a \leq 90°$. The difference between $T_{BH}(0°, a)$ and $T_{BV}(0°, a)$ was observed to decrease with a approaching 45° and/or with soil moisture content.

A numerical calculation based on a composite surface roughness – a small scale RMS height variations superimposed on a large periodic row structure – was made and found to predict the observed features within the model's limit of accuracy. It was concluded that the difference between $T_{BV}(0°, \alpha)$ and $T_{BH}(0°, \alpha)$ was due to the change in the local angle of field emission within the antenna field of view caused by the large-scale row structure.

17. Key Words (Selected by Author(s))	18. Distribution Statement		
19. Security Classif. (of this report) Unclassified	20. Security Classif. (of this page) Unclassified	21. No. of Pages	22. Price*

*For sale by the National Technical Information Service, Springfield, Virginia 22151.